Macro-heterogeneities in microstructures, solute concentrations, defects and tensile properties of high pressure die-cast Al-Mg-Si alloys

Shouxun Ji[1]*, Hailin Yang[1,2], Xiaopeng Cui[1,3], Zhongyun Fan[1]

1- Brunel Centre for Advanced Solidification Technology (BCAST), Institute of Materials and Manufacturing, Brunel University London, Uxbridge, Middlesex, UB8 3PH, UK.
2- State Key Laboratory of Powder Metallurgy, Central South University, Changsha 410083, China
3- Dept. of Mater Engineering, Changchun University of Technology, Changchun 130012, China

* Corresponding author, email: shouxun.ji@brunel.ac.uk

Abstract

The heterogeneities in tensile properties, microstructural characteristics, solute concentrations, and defects levels were studied for the castings with different thicknesses made by high pressure die-cast Al-Mg-Si alloys. For the local mechanical properties in the die-castings, the casting skin provided the highest, whereas the casting centre provided the lowest yield strength, UTS and elongation. The yield strength, UTS and elongation were significantly decreased towards the casting centre. The microstructural heterogeneity is characterised by the segregation of coarse fragmented dendrites, the reduction of solute concentrations of Mg and Si, and the increase of porosity level from the surface to the centre of castings. The growth velocities of eutectic α-Al phase estimated using the Jackson-Hunt model confirm that the growth variation is larger in the thin castings than that in thick castings.

Key words: Alloys; Microstructure; Mechanical properties; Solidification; Defects; Hetero-structures

1. Introduction

Heterogeneity is an inherent characteristic in as-cast microstructures because of their non-homogeneous chemistry, microstructure, defects, topology and the resultant mechanical properties in the different ranges of localization [1]. Generally, three types of heterogeneities characterise casting microstructures. The first category of heterogeneities is related to casting defects including shrinkage and gas porosity, misruns, cold shuts, inclusions, hot tears and hot spots. The second category of heterogeneities is related to the non-uniform microstructure from the surface to the centre of castings. The third category of heterogeneities is related to the non-uniform microstructure from the dendrites grown from primary solidification and the structure formed during the subsequent eutectic solidification in interdendritic regions. The chemical composition and the morphology between the primary dendrites and the interdendritic eutectics also differ in the as-cast microstructure. The first two categories are associated with macro-scale heterogeneity, but the third category is about micro-scale heterogeneity, which can be possibly eliminated through homogenization heat treatment. Obviously, the heterogeneity is different for the castings obtained from different casting processes.

High pressure die-casting (HPDC) is an extensively used casting process for manufacturing thin-wall components and lightweight structures [2,3]. The die-cast components have high heterogeneity compared to that produced by many other casting processes [4,5], which predominately originates from high speed and high turbulent melt flow during die filling, high cooling rate and two-stage solidification in HPDC [6,17]. This results in the formation of non-uniform microstructure and uncertain distribution of defects in die-castings. In general, the as-cast microstructure is significantly refined under high cooling rates, but is differentiated in several regions [7,8]. For instance, near the casting surface, fine grains form a defect-free layer, which is described as ‘the skin’ or ‘the surface layer’ [9,10, 18]. The zone located adjacent to the surface layer toward the centre, which provides an increased volume fraction of eutectic phase is usually defined as ‘the band zone’ [9]. In the central region, a bimodal grain microstructure consisting of a mixture of fine grains solidified inside the die cavity and coarse grains formed due to the external solidification in the shot sleeve (denoted as ESGs) is usually observed over the cross section of castings. The segregation of ESGs in the central region characterises the variation of the microstructure in die-castings. On top of the accumulation of ESGs, the central region always contains the increased levels of defects

such as porosities and inclusions, and the intermediate phases. For many years, the phenomenological study about microstructure and mechanical properties continues to cover a variety of die-cast alloys, including Al-Si, Al-Si-Cu, Al-Mg-Si alloys [11,12] and other alloys [13]. The literatures on the heterogeneity subject largely involve the effect of defects, gating system and casting parameters [6,14,15], solidification and microstructural evolution [16,17], the effect of skin [18], the identification of various phases [19,20], concentration profiles in the castings [21], quality mapping [22,23], the relationship between microstructure and mechanical properties under different casting conditions and under different heat treatments [24, 25]. Because of the heterogeneity in as-cast microstructure, the initialisation of deformation and the deformation levels at different locations is likely to be different. However, it is still lack of information on what the mechanical properties are at different locations in castings. No direct quantitative determinations of the non-uniform yield strength, ultimate tensile strength (UTS) and elongation at different points on the cross section of castings, especially regarding the relationship among the microstructure, solute concentrations, defect levels and the mechanical properties at different locations. In order to consolidate the knowledge in alloy selection and component design, it is essential to quantitatively find out and understand the heterogeneity in mechanical properties, microstructure, solute concentrations, and defect levels on the cross section of castings.

In the present paper, the die-cast rectangular tensile samples with different thicknesses were studied for the characteristics in microstructure, porosities, solute concentrations, and mechanical properties. A number of 2mm thick samples were obtained by machining 3mm and 5mm thick samples at different locations, and the mechanical properties were examined and compared with directly cast samples in associated with the local microstructure, solute concentrations and porosities. In discussion, the relationship among heterogeneity, solidification and mechanical properties were focused. The growth velocity of eutectic α-Al phase was estimated using the Jackson-Hunt model for different locations in the casting samples.

2. Experimental

The experimental casting samples of Al-Mg-Si alloys were made using commercial ingots of Al-50wt.%Si, pure Al and Mg. During the experiments, a clay-graphite crucible was used to melt 40kg alloys in an electric resistance furnace at 750^{o}C. Each element was added into the crucible with a specific ratio. The melt was degassed by a commercial rotatory degasser with

N_2 at 500rpm for 3 minutes. One mushroom casting sample with ϕ60×10mm testing part was made by casting the melt directly into a steel mould for composition analysis. 3 mm was cut off from the bottom of the sample before performing composition analysis using an optical mass spectroscopy, in which at least five spark analyses were carried out and the average value was taken as the chemical composition of the alloy. The measured compositions of the experimental alloy are 7.5±0.4wt.%Mg and 2.4±0.3wt.%Si with the balance Al and inevitable impurities.

After composition analysis and skimming, the melt was manually dosed and subsequently released into the shot sleeve of a 4500kN cold chamber HPDC machine for making ASTM standard tensile samples. The pouring temperature was 650^{o}C, measured by a K-type thermocouple. Six samples (3 of ϕ6.35mm and 3 rectangular samples with a cross section of 2×6.35, 3×6.35 and 5×6.35 mm, respectively) were made in each shot, but only the rectangular samples were used in this study. The metallic casting die was heated by the circulation of mineral oil at 250^{o}C. All castings were kept at ambient condition for at least 24 hours before performing the mechanical property test.

The tensile samples were randomly divided into two groups for each thickness. One group was for direct mechanical testing and microstructural analysis. Another group was used to machine new samples at different locations on the cross section. Fig. 1 shows the die-cast rectangular samples with 2, 3 and 5mm thick and the locations of the 2 mm thick rectangular samples machined from the 3mm and 5 mm thick die-cast samples. The distance from the casting centre is defined as the central line distance between the machined samples and the original die-cast samples, which is frequently used in the following description. The tensile tests were conducted following the ASTM B557 standard using an Instron 5500 Universal Electromechanical Testing Systems equipped with Bluehill software and a ±50kN load cell. All the tests were performed at ambient temperature (~25^{o}C). The gauge length of the extensometer was 25mm and the ramp rate for extension was 2mm/min. Each data reported is based on the properties obtained from 20 to 25 samples of direct die-casting samples and 5 to 10 of machined samples without showing obvious casting defects on the fractured surfaces.

The specimens for microstructure and porosity examination were cut from the middle of each tensile test sample. The microstructure and porosity was examined using a Zeiss optical microscopy with quantitative metallography, and a Zeiss Supra 35VP scanning electron microscopy (SEM) equipped with EDX. The porosity was measured on an unpolished sample

without etching. The porosity, grain size, and the volume fraction of the solid phase were measured using an AxioVision 4.3 Quantimet digital image analysis system. Five point analyses on the selected fields were conducted and the average was taken as the measurement.

3. Results

3.1 Heterogeneity in mechanical property

Fig. 2 shows the mechanical properties of the die-cast rectangular samples with different thicknesses. It is seen that the yield strength was slightly decreased but the UTS and elongation were increased with increasing the sample thickness. When the sample was 2mm thick, the yield strength, UTS and elongation were 177.1MPa, 302.1MPa and 6.7%, respectively. However, when the sample thickness was increased to 5mm, the yield strength was decreased to 168.9MPa, but the UTS and elongation were increased to 350.2MPa and 9.6%, respectively. The decrease of the yield strength was only 4.5%, but the increment of the UTS and elongation was 16% and 40%, respectively, when the sample thickness was increased from 2mm to 5mm, confirming that the increase of casting thickness was beneficial for the UTS and elongation with a slightly sacrificing the yield strength.

In order to investigate the heterogeneity in the mechanical properties of die castings, a number of 2mm thick rectangular samples were machined from the 3 mm and 5 mm thick rectangular castings. The detailed locations were schematically shown in Fig. 1. The tensile properties of 2 mm thick machined samples at different locations are shown in Fig. 3. When machining the 3mm thick castings, only two 2mm thick rectangular samples could be obtained, one was in the middle with two machined surface (denoted as casting centre in Fig. 3a) and the others was at the casting surface with one machined surface (denoted as casting skin in Fig. 3a). The yield strength, UTS and elongation of the samples at the casting centre were 167.4MPa, 310.6MPa and 6.3%, respectively, but they were 175.3MPa, 325.7MPa and 8.9% for the samples at the casting skin. The variation was 5% for the yield strength and UTS but 41% for the elongation. The results confirmed that the casting skin was significant for property enhancement, particularly for the elongation of die castings.

The similar observations were also found in the 2mm samples machined from 5mm thick castings. The mechanical properties are shown in Fig. 3b for the samples at different locations. As seen, four 2mm thick samples could be obtained from 5 mm thick castings with

0.5 mm intervals of locations. The variation of mechanical properties was significant from the surface to the centre of castings. The yield strength, UTS and elongation at the casting centre were 167.3MPa, 321.4MPa, and 7.3%, but those at the casting skin were increased to 175.5MPa, 346.8 MPa and 13.2%, respectively. The increment was 8% for the UTS, 5% for the yield strength, and 80% for the elongation. It is important to note that the machined samples from the 5mm thick casting surface provided very similar yield strength, but significantly improved UTS and elongation in comparison with those from the 3mm thick casting surface. The variation was 7% for the UTS and 48% for the elongation between the skin samples obtained in the 3mm thick castings and the 5mm thick castings. Moreover, three observations were obvious from the experimental results. (1) The thickness of samples could significantly differentiate the tensile properties of the die-castings. (2) The machined samples from the casting skin provided higher yield strength, UTS and elongation than those from the casting centre. (3) Tensile properties were different at the same location in different thick castings. Therefore, the heterogeneity in the mechanical properties was significant in the experimental alloy and castings.

3.2 Microstructural heterogeneity

Fig. 4 shows the as-cast microstructure on the cross section of rectangular die-cast samples. Similar to the microstructures observed in different alloys with different shape castings [5,7], the microstructures exhibited the typical three zones in all the samples with different thicknesses. Solute-enriched bands were observed parallel to the casting surfaces and to separate the skin and the central region of the castings. It is seen that the skin region was thicker in the 2mm thick samples than that in the 3mm and 5mm samples, indicating that the thinner casting wall may result in a thicker skin as the ingate size and filling velocity are the same for these rectangular castings. Further detailed studies of the microstructure are shown in Figs. 5 to 7 for different samples. The segregation of primary α-Al phase was apparent and more ESGs were found in the central region on the cross section. At the local area where the tensile samples were taken, two types of primary α-Al phases were seen in the centre region in all the samples, but ESGs were rarely observed in the skin region. The quantitative analysis in Fig. 8 showed that the volume fraction of the primary phase was at a level of 68% in the centre and 40% in the skin of casting samples. The coarse primary phase (α_1) was almost free from the casting surface and was gradually increased from the surface to the central region. The variation was up to 30% in the experimental samples, which represented

the significant heterogeneity in casting microstructure. This phenomenon was also observed in the samples with different thicknesses. The analytical results of grain sizes are shown in Fig. 9a, in which the coarse grains (α_1) became smaller near the casting skin than that in the casting centre, but the fine primary grains (α_2) showed no visible variations in size. The fine α-Al phase exhibited similar sizes from the surface to the centre of castings with different thicknesses. By combining the grain size and the volume fraction, the calculated overall grain sizes are shown in Fig. 9b for the experimental alloys. The grains sizes were obviously larger in the casting centre and smaller in the casting skin. However, the grain sizes of the primary α-Al phase were at similar levels at the skin and the centre of different samples.

The microstructural heterogeneity was also observed from the eutectic phase. The eutectic microstructures of die-cast samples with different thicknesses are shown in Fig. 10. Clearly, the finer eutectic microstructure was observed in the casting skin in comparison with that in the casting centre. In the meantime, it is also seen that the eutectic microstructure in the casting centre was finer for the as-cast sample with 2mm thickness than that of the 5 mm samples. This was confirmed by the detailed quantitative analysis shown in Fig. 11. The eutectic phase exhibited a higher volume fraction near the casting skin and a lower volume fraction in the casting centre. However, the eutectic spacing was significantly larger in the casting centre than that at the casting skin. It is noted that the eutectic spacing was at a similar level of 0.23 to 0.25μm at the casting skin for the samples with three thicknesses, but the eutectic spacing at the casting centre was varied from 0.38 μm for the 2 mm thick sample to 0.48 μm for the 5mm thick sample.

3.3 Composition heterogeneity

Fig. 12 shows the solute composition profile on the cross section of the rectangular tensile samples with different thicknesses. The concentrations of solute Mg and Si were generally consistent in the skin region but with a gradual drop toward to the centre inside the band. For instance, the Mg concentration was close to the nominal composition of 7.5wt.% in the skin region and gradually decreased to 6.4wt.% at the casting centre. Similarly, the Si concentration was also close to its nominal composition at 2.4wt.% in the skin region but slightly lower in the central region. However, the solute elements showed an apparent increase in the band zone. Mg and Si were enriched to 11.8wt.% and 3.3wt.%, respectively. Obviously, the peak of the solute enrichment in the band zone was much higher than the nominal composition in the alloy. The results confirmed the existence of significant

segregation and non-uniform distribution of the solute elements on the cross section of die-castings.

3.4 Porosity heterogeneity

Fig. 13 shows the porosity distribution on the cross section of the rectangular tensile samples with different thicknesses. A significant difference of the porosity levels was found between the skin region and the central region. The levels of porosity were increased from the skin to the centre of casting samples. It was less than 0.3% of porosity in the skin region, but over 1% of porosity in the central region. Therefore, heterogeneity in porosity levels was significant in the die-cast samples.

4. Discussion

4.1 Heterogeneity and Solidification

In all the casting process, melt is cooled down to form as-cast microstructure. Therefore, the heterogeneity in castings is essentially associated with solidification process. Unlike the conventional solidification process, in which the microstructure is normally initiated from the skin (the interface between mould and melt) and the solid phases gradually grows into the melt with different levels of undercooling, the solidification in high pressure die-casting occurs in two stages in the shot sleeve and in the die cavity. The solidification in the shot sleeve is under a conventional way to form a solid layer at the bottom of the shot sleeve, which is mostly likely broken and smashed and mixed with liquid during the forward movement of piston. The mixtures of solid and liquid phases are further being sheared when passing through the ingate and filling the die cavity. During die filling, the ESGs are experienced a pressure driven flow with high speed and high turbulence. Because the shear rate near the casting skin is close to zero and that at the central region are significantly higher according to the fundamental theory [26], the ESGs are therefore suffered sheared-induced migrations from the skin towards the casting centre. These results in a suspension of the segregated ESGs in the melt at the moment of finishing the fulfilment of die cavity, which is different to the melt with relatively homogeneous dispersion near the ingate. It needs to emphasise that the melt flows are throughout the whole die cavity and stopped in overflows. Therefore, the segregation of ESGs exists in whole castings. The liquid temperature after shearing during die filling is supposed to be uniform and without a significant superheat. The melt starts solidification immediately after die filling. Because the ESGs have a temperature

lower than the melting point of the alloy, the liquid surrounding the ESGs is essentially undercooled at the moment of fulfilling the die cavity. As a result, the solidification of the remnant liquid happens simultaneously throughout the die cavity, forming a number of fine grains in the form of globular particles or fine dendrites. The primary α-Al phase formed in the die cavity shows less significant heterogeneity because of the fine grain sizes. Meanwhile, as the shear rate at the casting skin (mould or die surface) is zero in principle, the melt is thus stuck on the die surface at the first moment of die filling. The melt away from the mould surface continues the filling process, forming a dynamic balance between the static skin and the turbulent flow in the inner channel. Therefore, the microstructure in the skin region has different morphology to that in the central region. Moreover, the rapid solidification for the segregated mixture of the ESGs and melt inside the die cavity will restrain the release of the gas introduced by turbulence in the melt. Consequently, the porosity in the casting central region is higher than that in the skin region.

4.2 The estimation of eutectic growth velocity

As mentioned previously [17, 20], the eutectic solidification happens after fulfilling the die cavity. Because the solidification inside the die cavity also includes the formation of primary α-Al grains, the eutectic reaction is supposed to occur under a static condition and confined to the small intergranular areas. From the experimental results, the eutectic spacing from the casting skin to the casting centre is slightly different, indicating the cooling rate is different during solidification. The high cooling rate is able to lead the formation of fine eutectic spacing and the size of eutectic cells. Currently, the direct measurement of the cooling rate in the die cavity is still very difficult, in particular for the variation of cooling rate on the cross section of thin wall die-castings. Therefore it is worth of estimating the difference of cooling rates using the easily measured eutectic spacing.

According to the Jackson-Hunt theory of eutectic growth [27], the relationship between eutectic spacing λ and growth velocity V follows

$$\lambda^2 V = constant \qquad (3)$$

Although the Jackson-Hunt theory is generally suitable for most eutectic reactions, the determination of the constant is still a challenge and the results vary from one to another from the published literatures. Table 1 shows the data of constant used in published papers carried out by Grugel & Kurz [28], Böyük et al. [29], Kaya et al. [30], Whelan & Haworth [31],

Trivedi et al. [32], Moore & Elliot [33], Cadirli et al. [34,35] Koçak et al. [36]. Because no accurate data was found for AlMgSi alloys, it is expected that the constant at a range of 130-160 μm^3/s is approximately acceptable. When $\lambda^2 V$ = 130 to 160 μm^3/s, we can obtain the different growth velocities with the variation of λ from the skin to the centre of die-castings. Therefore, the possible growth velocity for the different thick samples can be calculated using the measured eutectic spacing. The results are shown in Fig. 14, in which a band provides the growth range for each casting thickness. The typical growth velocity at the skin and the centre is 2625 μm/s and 750 μm/s for the 5mm thick casting, 2740 μm/s and 820 μm/s for the 3mm thick casting, and 2865 μm/s and 1004 μm/s for the 2 mm thick casting, respectively. It is understandable that the variation of the growth velocity is larger for the thin casting than that of the thick castings. However, the growth velocities near the casting surface are very close for the different castings. And, the variation of growth velocity from the skin to the centre is much less for the 5mm thick castings than that for the 2 mm thick castings.

Generally, the growth velocity is proportional with the undercooling in the melt, which is significantly affected by the cooling rate of solidification [1, 37]. A high cooling rate always results in a large undercooling. At a large undercooling, the number of nuclei that can grow up in the melt during nucleation is increased, leading to form the increased number of eutectic cells and the decreased cell sizes during solidification. Meanwhile, the growth is controlled by solid-liquid interface movement through the redistribution of solute in front of the interface. The high cooling rate can form an increased thermal gradient in front of the solid-liquid interface, by which the diffusion is promoted and therefore the growth velocity steeply rises during solidification.

4.3 The microstructural heterogeneity and mechanical properties

The non-uniform microstructures under as-cast condition show different behaviours under stress. From the macro scales, the stress distribution on the cross section is not uniform due to the segregation of the primary α-Al phase and high concentrate of solute in the band zone. From the micro scales, the local stresses are expected to be different in the different phases. The stress concentrations are increased around hard particles/phases that cause additional plasticity in its vicinity. The high localized stress may promote the formation of high dislocation concentration in the eutectic regions much more than in the centre of the primary α-Al phase. Thus, the deformation should be localized. The significantly more deformation occurs in the α-Al phase, in particular at or near the dendrite/grain boundaries to compensate

the less deformation of eutectic Mg_2Si and intermetallics. Because of the higher stress concentrations at the boundaries and the lamellar microstructure of eutectic, the primary and eutectic α-Al phase largely controls the mechanical properties of Al-Mg-Si alloys. Accordingly, solution strengthening of the α-Al phase should be the basis of any material design strategy to enhance die-cast Al-Mg-Si alloys. Both the eutectic α-Al phase and the primary α-Al phase in the vicinity of dendrite/grain boundaries need to be strengthened. The morphology of the eutectic intermetallic phases also plays an important role because the intermetallics precipitate in the eutectic region in which the α-Al phase is soft. The intermetallic Mg_2Si phase is typically hard to deform as they exhibit strong covalent bonds. As shown in the experimental results, the morphology of the eutectic Mg_2Si phase is very fine under the high cooling rate during solidification. The soft α-Al phase and the intermetallic phases are sandwiched in the microstructure. This should provide a higher strength.

5. Conclusions

a) Macro-heterogeneities in microstructure, solute concentrations and defect levels strongly affect the as-cast tensile properties of Al-Mg-Si alloys. Under the same ingate velocity and overflow, the 2 mm die-cast samples provide slightly higher yield strength and lower UTS and elongation than the 3 mm and 5 mm die-cast samples. For the local mechanical properties on the thick die-castings represented by the machined 2 mm thick samples, the casting skin provides the highest, whereas the casting centre provides the lowest yield strength, UTS and elongation. The yield strength, UTS and elongation are significantly decreased towards the casting centre.
b) The heterogeneities in microstructure are mainly characterised by the significant segregation of ESGs from the surface to the centre of castings, although the primary α-Al phase and the eutectic Al-Mg_2Si phase solidified in the die cavity also show a slight difference in terms of grain size and eutectic spacing.
c) The heterogeneities in solute concentrations are mainly characterised by the slight decrease of Mg and Si contents from the casting skin towards the casting centre, and a high peak in the band zone.
d) The heterogeneities in porosity levels are mainly characterised by the significant decrease from the centre to the surface of the die-castings, which may be the predominant factor to affect the tensile strength of the die-castings.

e) The growth velocity of eutectic α-Al phase can be calculated using the Jackson-Hunt model. The results confirm that the variation of growth velocity is larger in the thin castings than that in thick castings. However, the growth velocities near the surface are close in the different thick castings.

Acknowledgements

The financial support is gratefully acknowledged for the Engineering and Physical Sciences Research Council (EPSRC) (Project number: EP/1038616/1), Technology Strategy Board (TSB) (Project number: 101172), United Kingdom.

References

[1] J. Campbell, Castings, 2nd edition, Butterworth Heinemann, Oxford, United Kingdom, 2003.

[2] E. J. Vinarcik, High integrity die casting processes, John Wiley & Sons, New York, 2003.

[3] H. L. MacLean, L. B. Lave, Evaluating automobile fuel/propulsion system technologies, Progress in Energy and Combustion Science 29 (2003)1-69.

[4] S. Ji, D. Watson, Z. Fan, M. White, Development of a super ductile die-cast Al–Mg–Si alloy, Mater. Sci. & Eng. A 556(2012) 824 -33.

[5] S. Otarawanna, C.M. Gourlay, H.I. Laukli, A.K. Dahle, Microstructure formation in AlSi4MgMn and AlMg5Si2Mn high-pressure die castings, Metall. Mater. Trans. A 40A(2009)1645-59.

[6] M.R. Barone, D.A. Caulk, Analysis of liquid metal flow in die casting. Int. J. Eng. Sci. 38 (2000) 1279-1302.

[7] A. K. Dahle, D. H. StJohn, Rheological behaviour of the mushy zone and its effect on the formation of casting defects during solidification, Acta Mater. 47(1999)31-41.

[8] C. M. Cepeda-Jiménez, A. Orozco-Caballero, J. M. García-Infanta, A. P. Zhilyaev, O.A. Ruano, F. Carreño, Assessment of homogeneity of the shear-strain pattern in Al–7 wt%Si casting alloy processed by high-pressure torsion, Mater. Sci. & Eng. A 597(2014)102-110.

[9] S. Otarawanna, C. M. Gourlay, H. I. Laukli, A. K. Dahle, The thickness of defect bands in high-pressure die castings, Materials Characterization 60(2009) 1432-1441.

[10] K. V. Yang, M. A. Easton, C. H. Cáceres, The development of the skin in HPDC Mg–Al alloys, Mater. Sci. & Eng. A 580(2013) 191-195.

[11] R. Kimura, H. Hatayama, K. Shinozaki, I. Murashima, J. Asada, M. Yoshida, Effect of grain refiner and grain size on the susceptibility of Al–Mg die casting alloy to cracking during solidification, J. Mater. Processing Tech. 209(2009)210-15.

[12] A. Hamasaiid, M.S. Dargusch, C.J. Davidson, S. Tovar, T. Loulou, F. Rezai-Aria, G. Dour, Effect of mould coating materials and thickness on heat transfer in permanent mould casting of aluminium alloys, Metall. Mater. Trans. A 38(2007)1303-15.

[13] K. V. Yang, C.H. Cáceres, A.V. Nagasekhar, M.A. Easton, The skin effect and the yielding behaviour of cold chamber high pressure die cast Mg–Al alloys, Mater. Sci. & Eng. A 542 (2012) 49– 55.

[14] P. K. Seo, D.U. Kim, C. G. Kang, Effects of die shape and injection conditions proposed with numerical integration design on liquid segregation and mechanical properties in semi-solid die casting process, J. Mater. Processing Tech. 176(2006) 45-54.

[15] P. W. Cleary, J. Ha, M. Prakash, T. Nguyen, Short shots and industrial case studies: Understanding fluid flow and solidification in high pressure die casting, Applied Mathematical Modelling 34(2010) 2018-2033.

[16] Y. Sui, Q. Wang, B. Ye, L. Zhang, H. Jiang, W. Ding, Effect of solidification sequence on the microstructure and mechanical properties of die-cast Al–11Si–2Cu–Fe alloy, J. Alloys and Compounds 649(2015) 679-686.

[17] S. Ji, Y. Wang, D. Watson, Z. Fan, Microstructural evolution and solidification behaviour of Al-Mg-Si Alloy in high-pressure die casting, Metall. Mater. Trans. A 44A(2013)3185-3197.

[18] Z.W. Chen, Skin solidification during high pressure die casting of Al–11Si–2Cu–1Fe alloy, Mater. Sci. & Eng. A 348(2003) 145-153.

[19] J. A. Taylor, Iron-containing intermetallic phases in Al-Si based casting alloys, Procedia Materials Science 1(2012) 19-33.

[20] S. Ji, W. Yang, F. Gao, D. Watson, Z. Fan, Effect of iron on the microstructure and mechanical property of Al–Mg–Si–Mn and Al–Mg–Si diecast alloys, Mater. Sci. &Eng. A 564(2013)130–139.

[21] S. Ferraro, A. Fabrizi, G. Timelli, Evolution of sludge particles in secondary die-cast aluminum alloys as function of Fe, Mn and Cr contents, Materials Chemistry and Physics 153(2015)168-179.

[22] N. Gramegna, I. Loizaga, S. Berrocal, F. Bonollo, G. Timelli, Advances in production management systems, competitive manufacturing for innovative products and services, IFIP Advances in Information and Communication Technology 397 (2013) 502-509.

[23] G. Timelli, F. Bonollo, Quality mapping of aluminium alloy die castings, Metallurgical Science and Technology 26-1 (2008) 2-8.

[24] R.N. Lumley, Progress on the heat treatment of high pressure die castings, Fundamentals of Aluminium Metallurgy, 2011 pp 262-303.

[25] G. Sha, H. Möller, W.E. Stumpf, J.H. Xia, G. Govender, S.P. Ringer, Solute nanostructures and their strengthening effects in Al–7Si–0.6Mg alloy F357, Acta Materialia 60(2012)692-701.

[26] P. R. Nott, J. F. Brady, Pressure-driven flow of suspensions, simulation and theory, J. Fluid Mech. 275 (1994)157-199.

[27] K.A. Jackson, J.D. Hunt, Lamellar and rod eutectic growth, Trans. Metall. Soc. AIME., 236(1966)1129-42.

[28] R. Grugel, W. Kurz, Growth of interdendritic eutectic in directionally solidified Al-Si alloys, Metall. Mater. Trans. A, 18(1987)1137-42.

[29] U. Böyük, S. Engin, N. Maraşlı, Microstructural characterization of unidirectional solidified eutectic Al–Si–Ni alloy, Materials Characterization 62 (2011)844-51.

[30] H. Kaya, E. Cadirli, M. Gündüz, Eutectic growth of unidirectionally solidified bismuth–cadmium alloy, J. Materials Processing Technology 183 (2007)310-20.

[31] E. P. Whelan, C. W. Haworth, J. Aust. Inst. Met. 12 (1967)77-126.

[32] R. Trivedi, J.T. Mason, J.D. Verhoeven, W. Kurz, Eutectic spacing selection in lead-based alloy systems, Metall. Mater. Trans. 22A (1991)2523-33.

[33] A. Moore, R. Elliott, Solidification of Metals, Proc. Conf. Iron and Steel Ins. Publ., Brighton, UK, 1967. pp. 167-74.

[34] E. Cadirli, H. Kaya, M. Gunduz, Effect of growth rates and temperature gradients on the lamellar spacing and the undercooling in the directionally solidified Pb–Cd eutectic alloy, Mater. Res. Bull., 38(2003)1457-76.

[35] E. Cadirli, A. Ulgen, M. Gunduz, Directional solidification of the aluminium-copper eutectic alloy, Mater. Trans. JIM. 40(1999)989-96.

[36] Y. Koçak, S. Engin, U. Böyük, N. Maraşlı, The influence of the growth rate on the eutectic spacings, undercoolings and microhardness of directional solidified bismuthelead eutectic alloy, Current Applied Physics 13 (2013) 587-593.

[37] D.M. Schwarz, C.B. Arnold, M.J. Aziz, D.M. Herlach, Dendritic growth velocity and diffusive speed in solidification of undercooled dilute Ni-Zr melts, Mater. Sci. & Eng. A 226-228 (1997) 420-424.

Table 1 The constant for the Jackson-Hunt model measured or calculated used in different papers.

Author	Alloys (wt.%)	Equation	Ref.
Grugel & Kurz	Al- 6~12Si	$\lambda^2 V$ = 625±9.6 μm³/s	[28]
Böyük et al.	Al-11.1Si-4.2Ni	$\lambda^2{}_{\mathrm{Si}} V$ = 158 μm³/s, $\lambda^2{}_{Al_3Ni} V$=63 μm³/s	[29]
Kaya et al.	Bi-Cd	$\lambda^2 V$ = 30.609 μm³/s	[30]
Kaya et al.	Bi-Cd	$\lambda^2 V$= 39.059 μm³/s	[30]
Whelan &Haworth		$\lambda^2 V$ = 19.6 μm³/s	[31]
Trivedi et al.	Pb based alloys	$\lambda^2 V$ = 21.1 μm³/s	[32]
Moore & Elliot		$\lambda^2 V$ = 21.8 μm³/s	[33]
Cadirli et al.	Pb–Cd	$\lambda^2 V$ = 23.7 μm³/s	[34]
Cadirli et al.	Al-Cu	$\lambda^2 V$=156 μm³/s	[35]
Koçak et al.	Bi-Pb	$\lambda^2 V$=104.5 μm3 /s	[36]

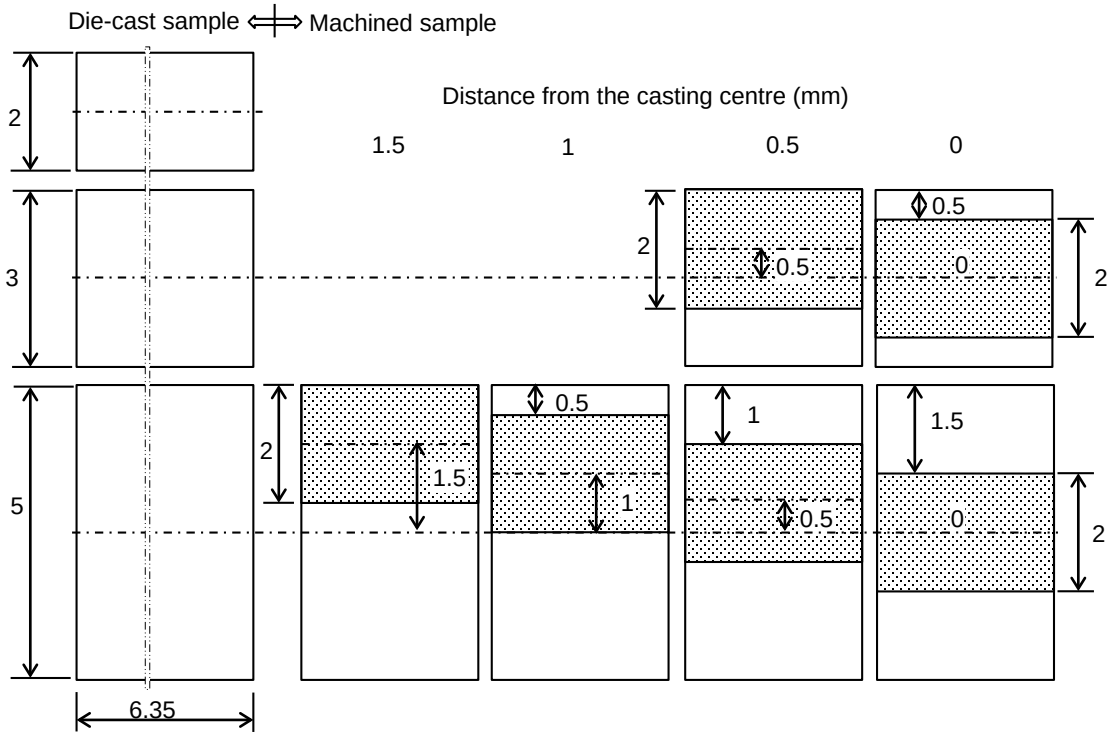

Figure 1 Schematic diagram showing the 2, 3 and 5mm thick die-cast rectangular samples and the locations of the 2 mm thick rectangular samples machined from the 3mm and 5 mm thick die-cast samples. The distance from the casting centre is defined as the central line distance between the machined samples and the original die-cast samples, which is frequently used in the following figures.

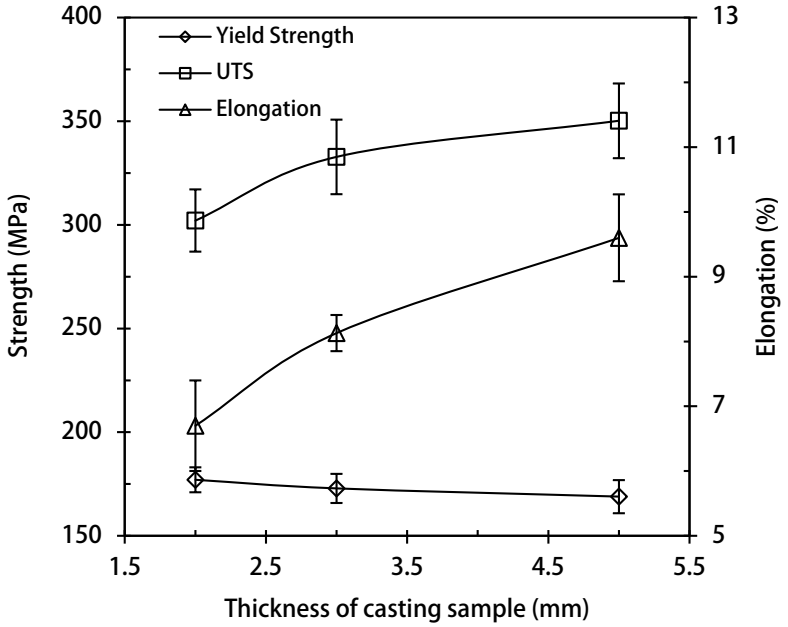

Figure 2 Effect of the thickness of die-casting rectangular samples on the tensile properties of the Al-7.5wt.%Mg-2.4wt.%Si alloys.

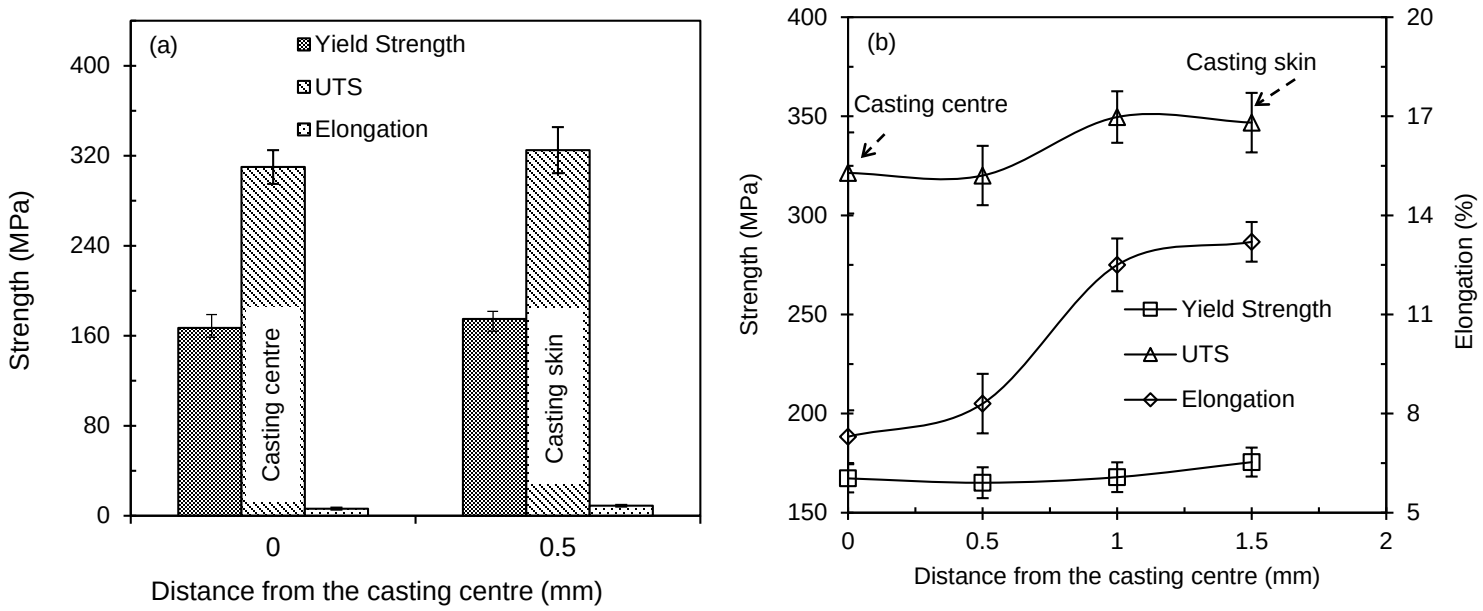

Figure 3 The tensile properties of the Al-7.5wt.%Mg-2.4wt.%Si alloy with different surface conditions and locations of the 2 mm thick rectangular samples machined from (a) 3mm thick rectangular casting samples and (b) 5mm thick rectangular casting samples.

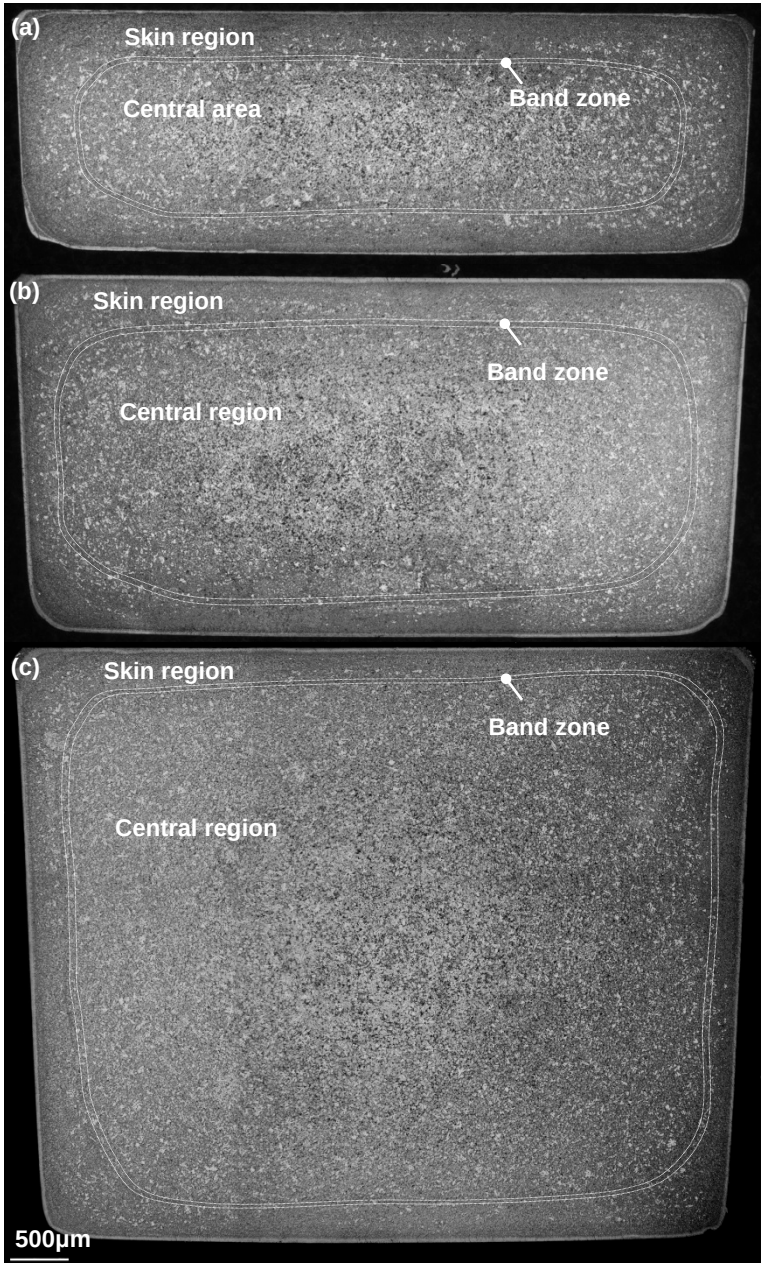

Figure 4 The microstructure on a cross section of the rectangular tensile samples made by the Al-7.5wt.%Mg-2.4wt.%Si alloy with different thicknesses, showing the skin region, band zone and central area.

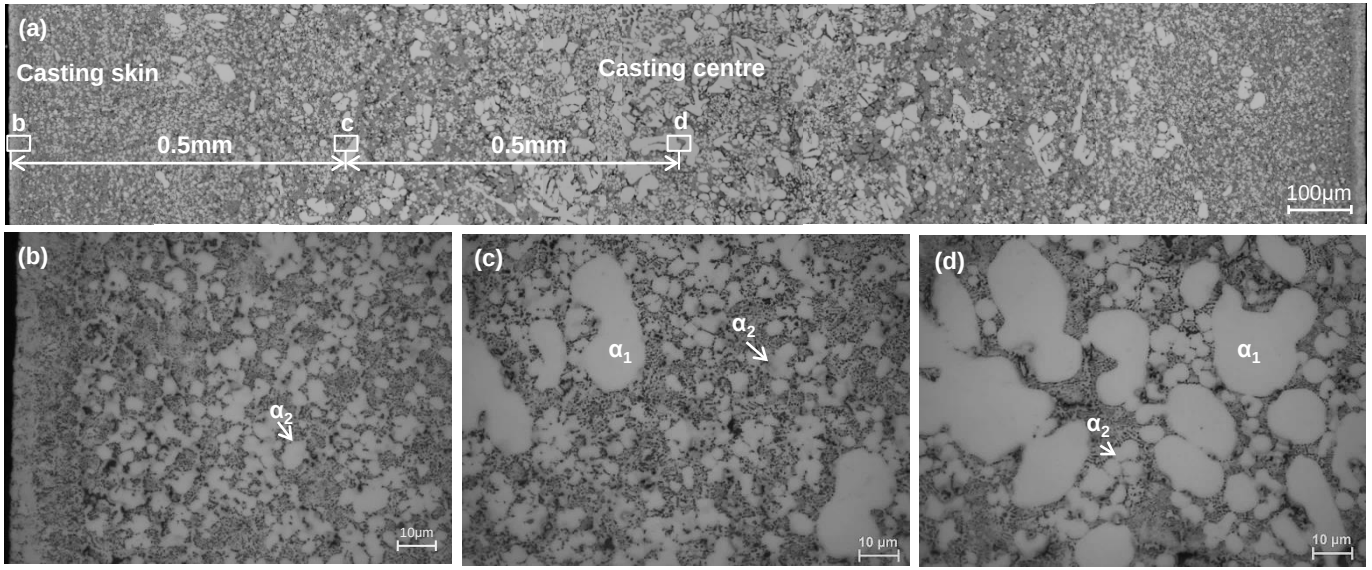

Figure 5 Optical micrographs showing the microstructure of the die-cast Al-7.5wt.%Mg-2.4wt.%Si alloy, (a) on a cross section of 2mm rectangular tensile sample, (b) on the skin, (c) 0.5mm from the casting centre, (d) in the centre.

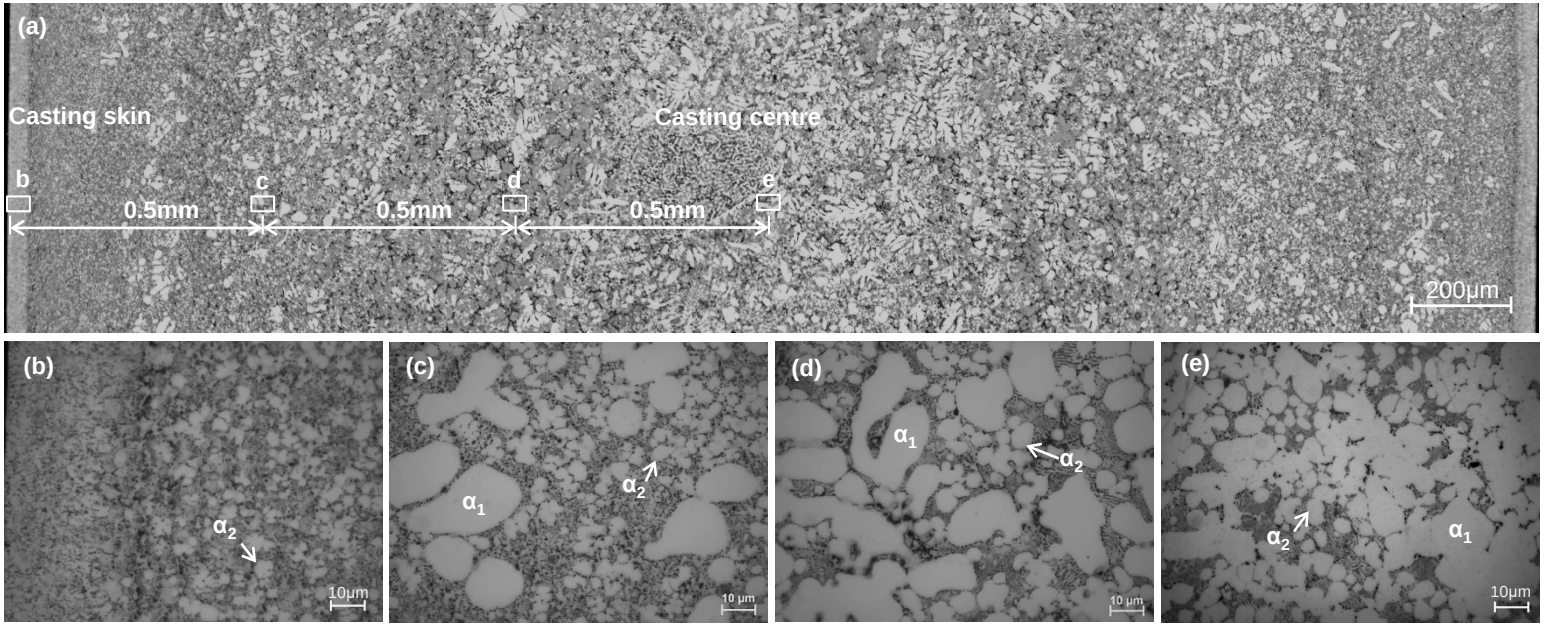

Figure 6 Optical micrographs showing the microstructure of the die-cast Al-7.5wt.%Mg-2.4wt.%Si alloy, (a) on a cross section of 3mm square tensile sample, (b) on the skin, (c) and (d) 0.5mm intervals from the casting centre, (e) in the centre.

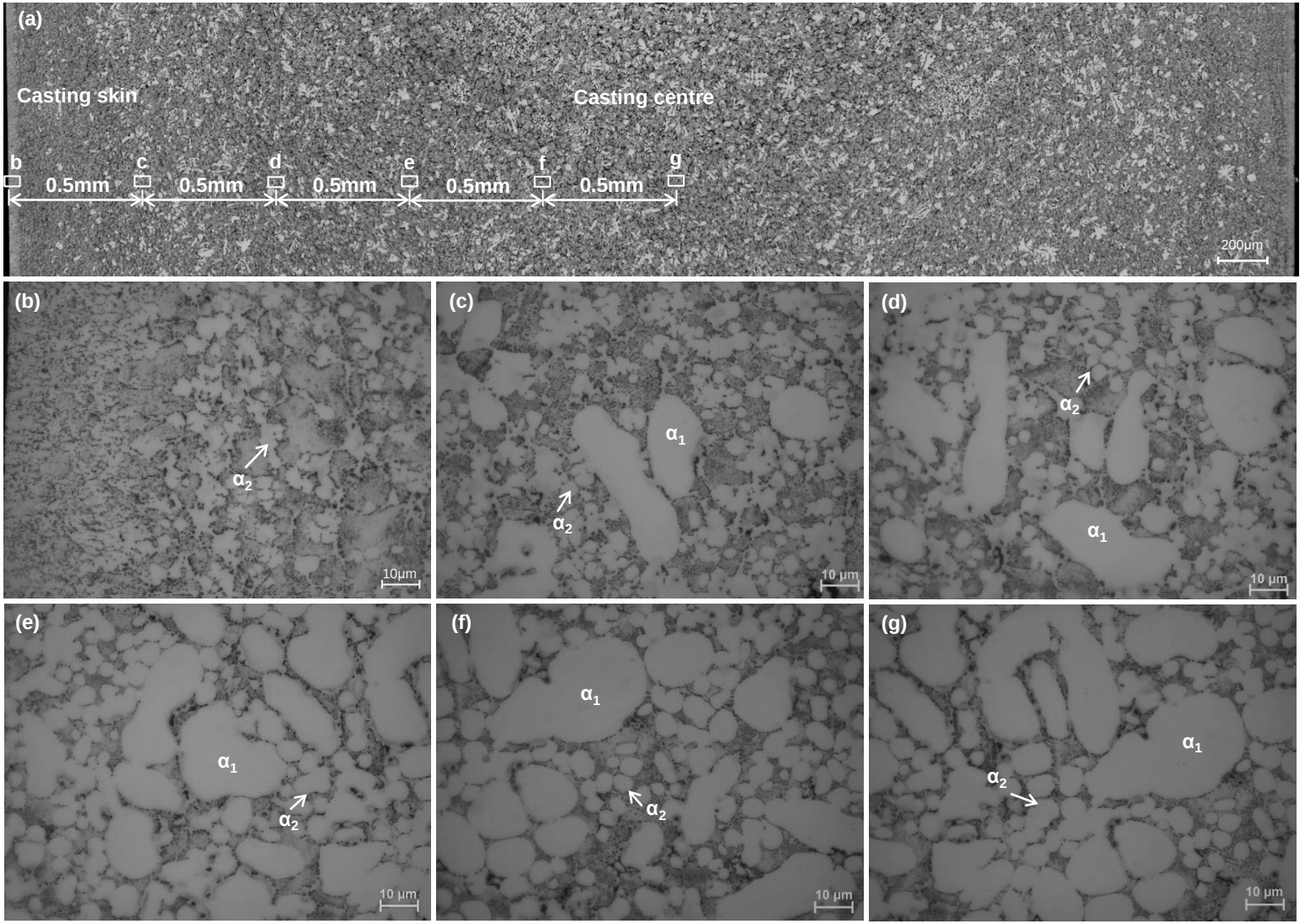

Figure 7 Optical micrographs showing the microstructure of the die-cast Al-7.5wt.%Mg-2.4wt.%Si alloy, (a) on a cross section of 5mm rectangular tensile sample, (b) on the skin, (c) to (f) 0.5mm intervals from the casting centre, (g) in the casting centre.

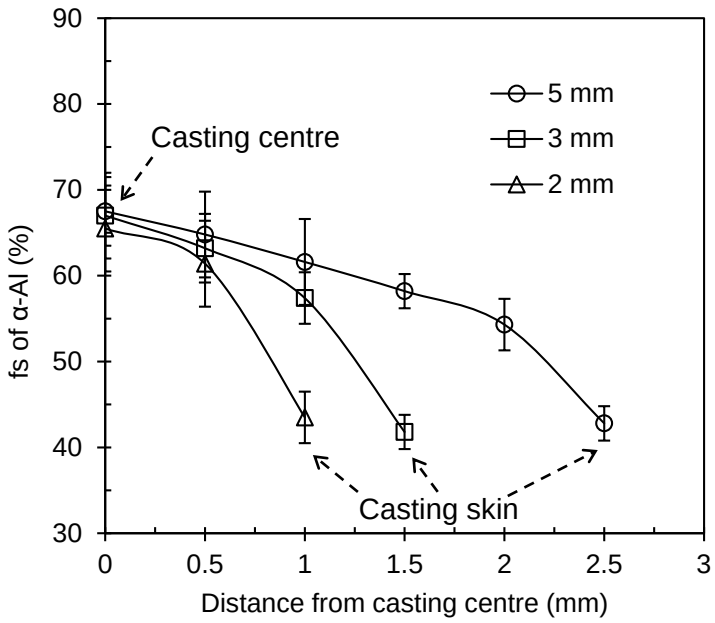

Figure 8 Volume fractions of the primary α-Al phase on the cross section of the die-cast Al-7.5wt.%Mg-2.4wt.%Si alloy with different thicknesses of rectangular tensile samples.

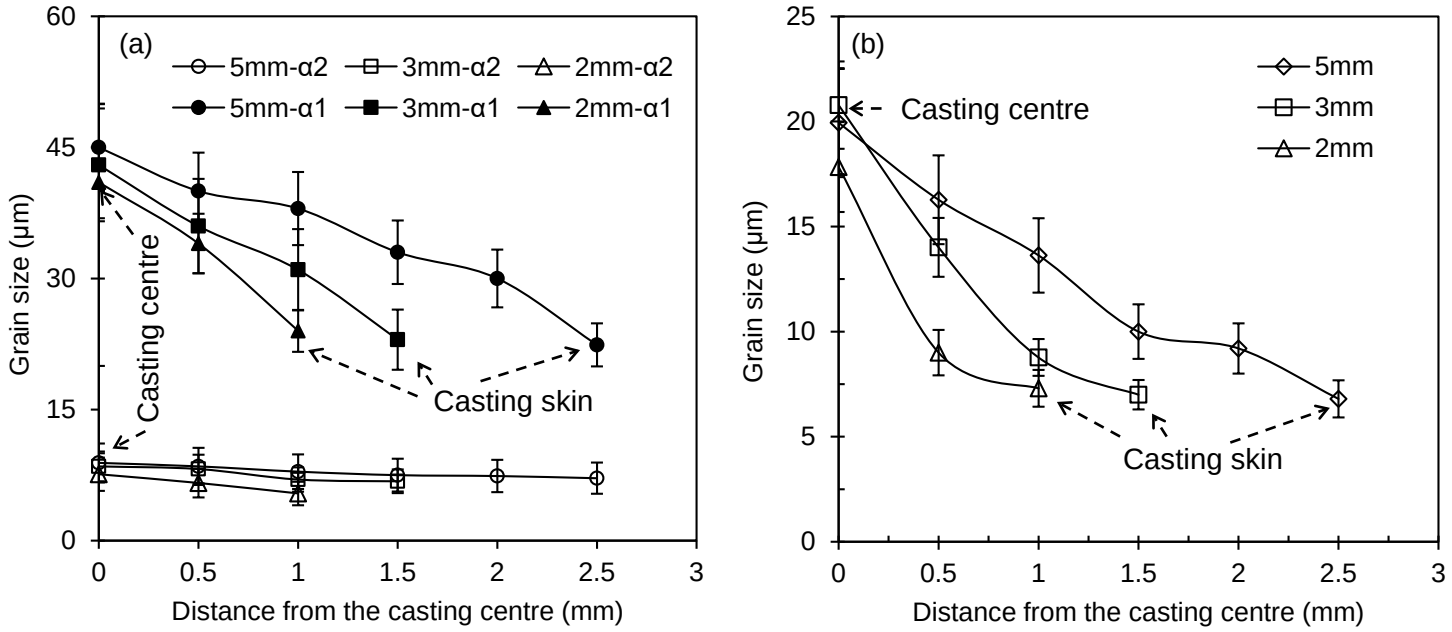

Figure 9 Grain sizes of the primary α-Al phase on the cross section of the die-cast Al-7.5wt.%Mg-2.4wt.%Si alloy with different thicknesses of rectangular tensile samples, (a) the average size of the coarse primary α-Al phase (α_1) and the fine coarse primary α-Al phase (α_2), (b) overall average size of the primary α-Al phase.

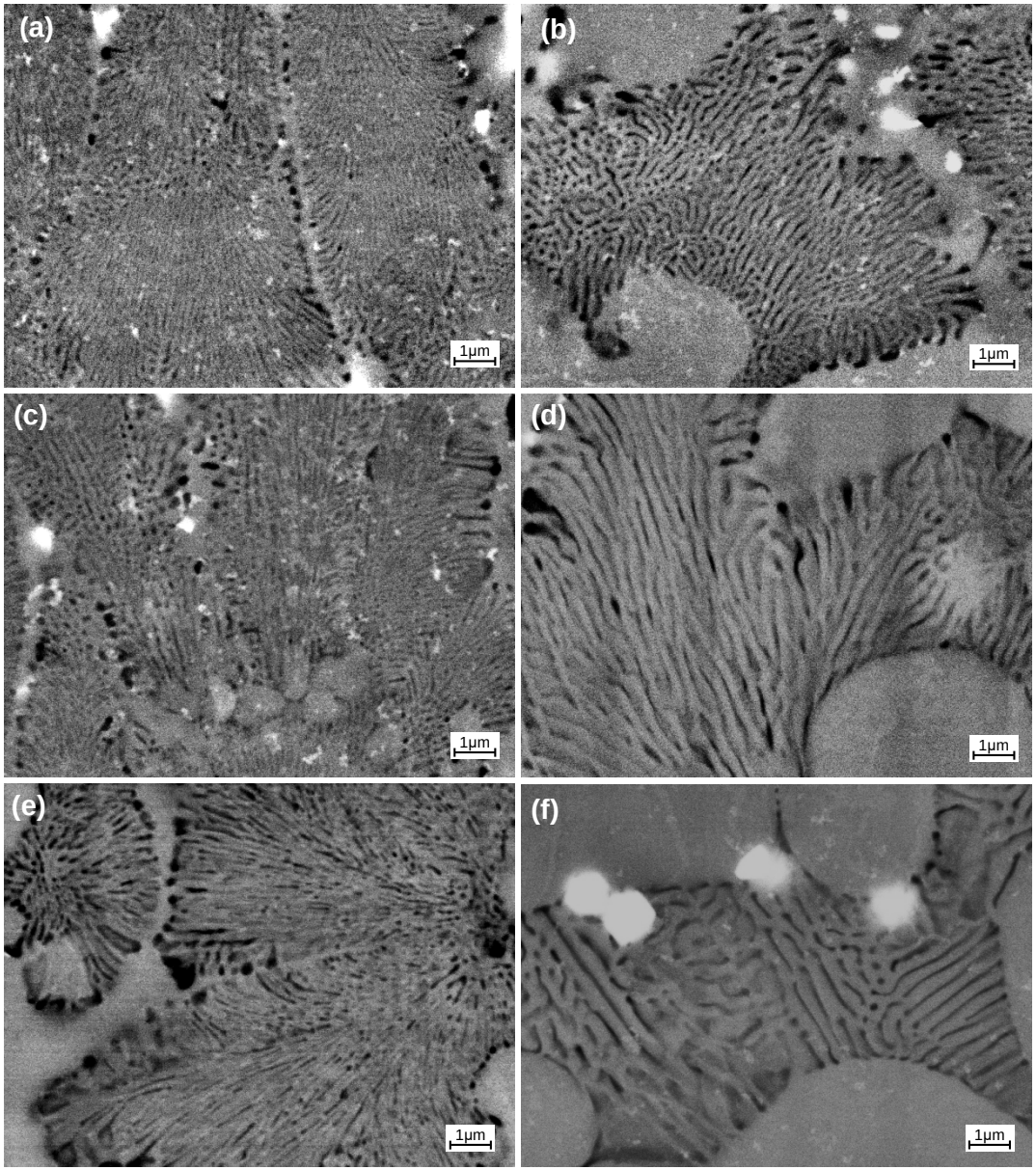

Figure 10 Backscattered SEM images showing the eutectic microstructure of (a) and (b) 2mm, (c) and (d) 3mm, and (e) and (f) 5mm thick rectangular tensile samples at the skin (a,c,e) and in the centre (b,d,f).

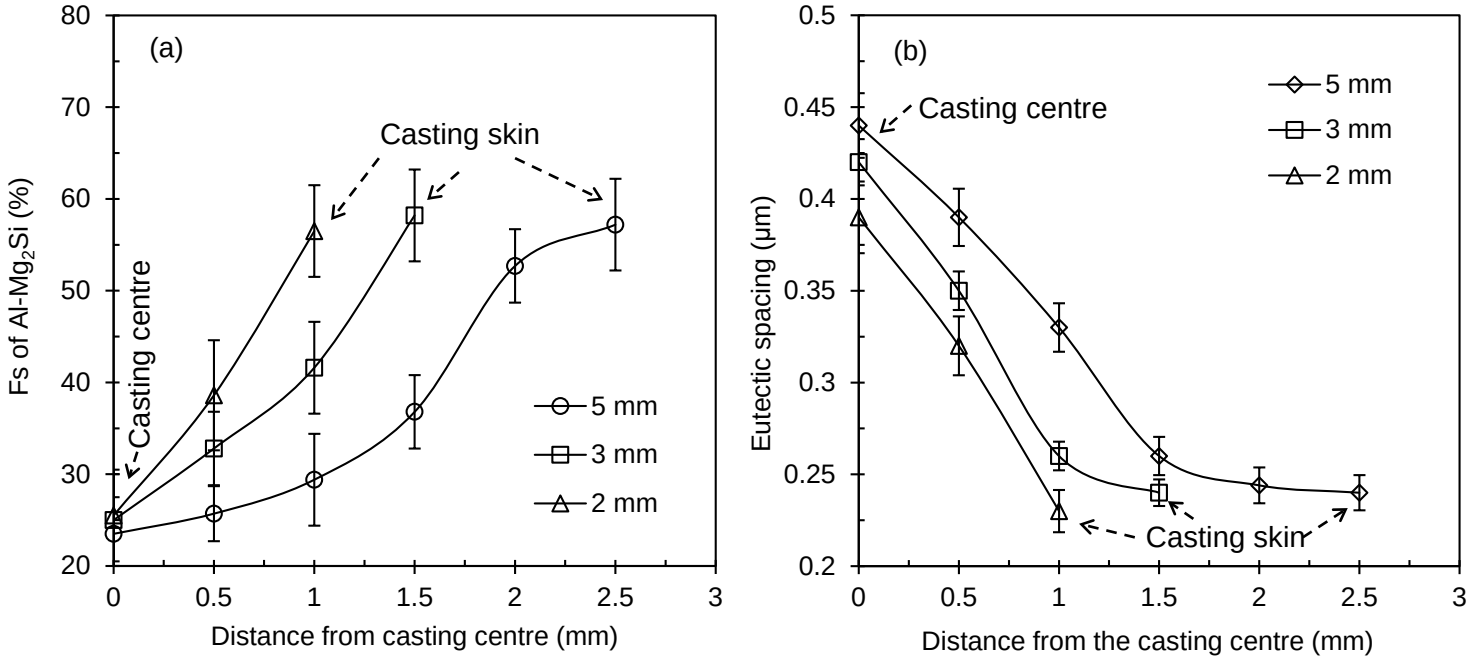

Figure 11 Measured (a) volume fractions and (b) the eutectic spacing of the eutectic Al-Mg_2Si phase on the cross section of the Al-7.5wt.%Mg-2.4wt.%Si alloy with different thicknesses of the rectangular tensile samples.

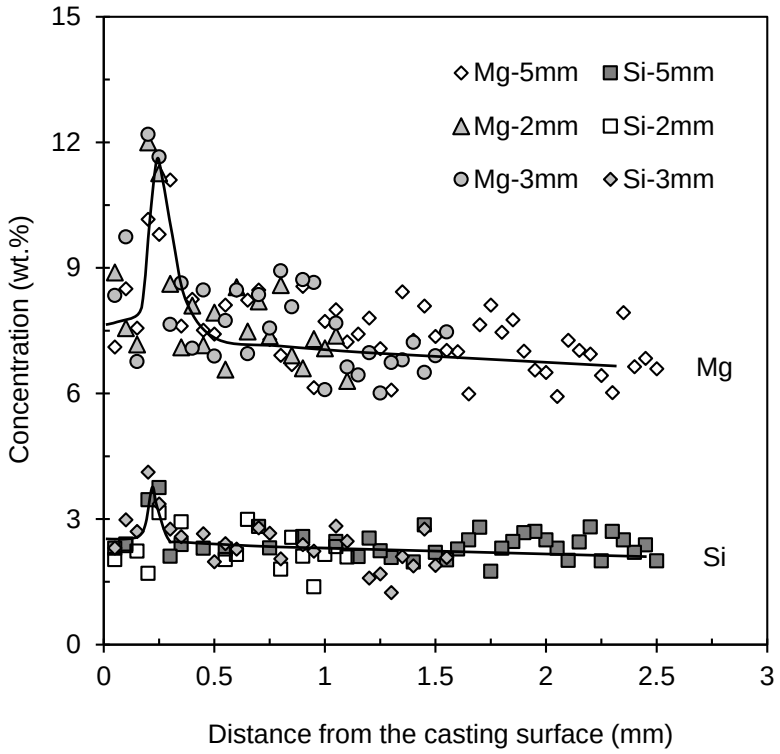

Figure 12 The distribution of Mg and Si elements measured on the cross section of the rectangular tensile samples made by the Al-7.5wt.%Mg-2.4wt.%Si alloy with different thicknesses.

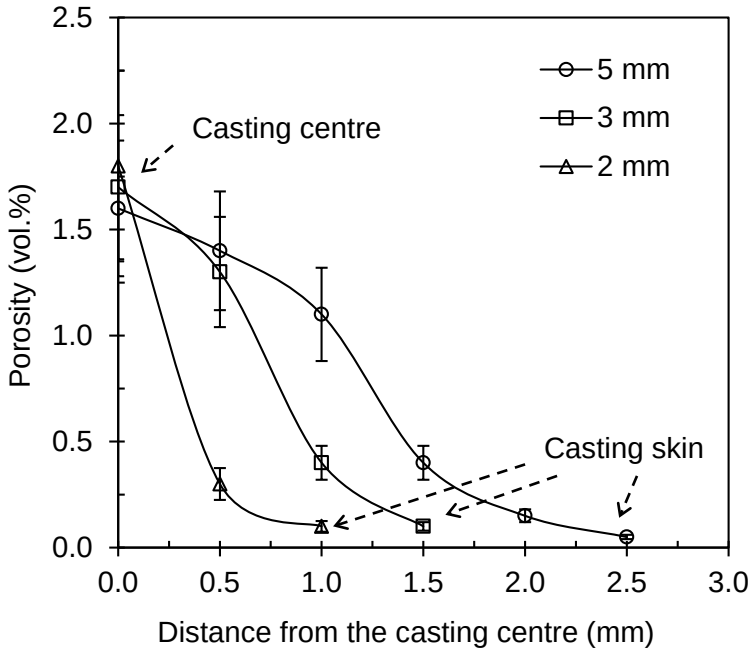

Figure 13 The distribution of porosity measured on the cross section of the rectangular tensile samples made by the Al-7.5wt.%Mg-2.4wt.%Si alloy with different thicknesses.

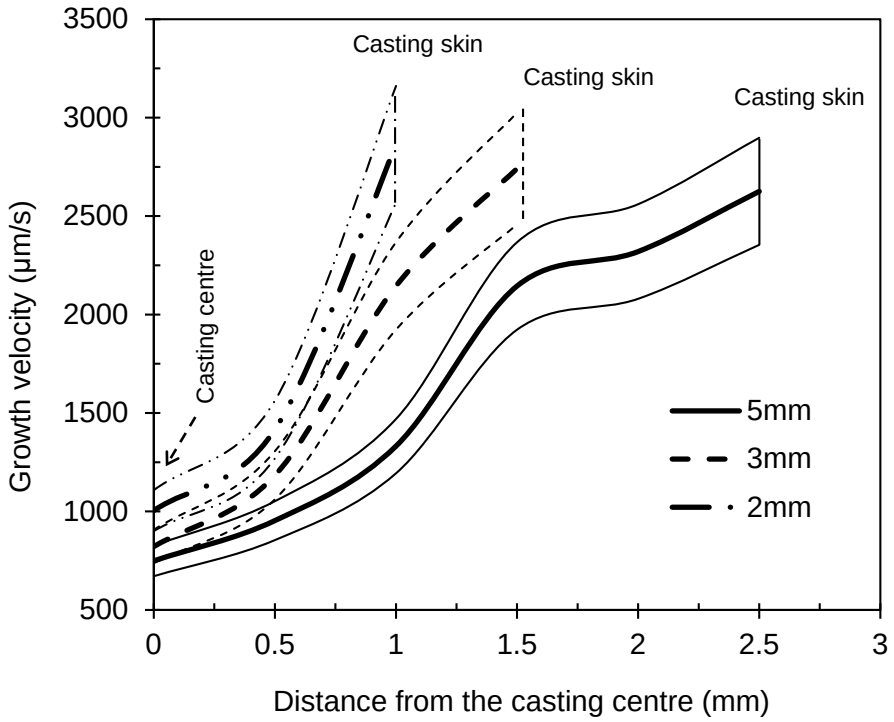

Figure 14 Calculated growth velocity of eutectic α-Al phase according to the eutectic spacing of α-Al phase on the cross section of the Al-7.5wt.%Mg-2.4wt.%Si alloy with different thicknesses of the rectangular tensile samples.